Chemical Engineering Journal 210 (2012) 510–519

Contents lists available at SciVerse ScienceDirect

Chemical Engineering Journal

journal homepage: www.elsevier.com/locate/cej

Activated carbon from carrot dross combined with magnetite nanoparticles for the efficient removal of p-nitrophenol from aqueous solution

Tahereh Rohani Bastami, Mohammad H. Entezari *

Department of Chemistry, Ferdowsi University of Mashhad, 91775 Mashhad, Iran

HIGHLIGHTS

- Activated carbon from carrot dross (AC) prepared, magnetized and used for removal of PNP.
- Magnetization of AC (MAC) was made by mixing AC with Fe_3O_4 sol in two mass ratios.
- Surface area of AC and MAC with two mass ratios were 447, 435, and 340 $m^2\ g^{-1}$, respectively.
- Batch sorption for AC and MAC carried out at different pH, contact time, and concentration.
- Magnetic property of MAC facilitates the separation of solid phase much easier than AC.

ARTICLE INFO

Article history:
Received 7 June 2012
Received in revised form 31 July 2012
Accepted 1 August 2012
Available online 14 August 2012

Keywords:
Carrot activated carbon
Magnetic carrot activated carbon
Surface oxygen groups
Ultrasonic irradiation
P-nitrophenol

ABSTRACT

Activated carbon from carrot dross (AC) was prepared, magnetized and used for the removal of p-nitrophenol from aqueous solution. The magnetization of AC was carried out by mixing the AC with diluted Fe_3O_4 sol in two different mass ratios of Fe_3O_4/AC. The characterization of both magnetized and original AC were studied by X-ray diffraction, Fourier transform infrared spectroscopy, scanning electron microscopy, surface area measurement, elemental analyses, zero point charge measurement, and vibrating sample magnetometer. The surface area measurement of AC and magnetic activated carbons of carrot dross (MAC) with two mass ratios of Fe_3O_4/AC (1/8 and 1/5) were 447, 435, and 340 $m^2\ g^{-1}$, respectively. Batch sorption studies for the AC and MAC were carried out at different pH values, solid to liquid ratios, contact times, and initial concentrations of the pollutant in the presence and absence of ultrasonic irradiation. The sorption isotherms were obtained in the range of 50–500 mg L^{-1}. The results for the AC and MAC in the absence of ultrasound and for MAC in the presence of ultrasound fit well with Freundlich isotherm. In contrast, the results for AC in the presence of ultrasonic irradiation fit well with Langmuir model. In the case of AC, the values of intraparticle diffusion rate constant in the presence of ultrasound were greater than conventional method. In the case of MAC, the presence of magnetite nanoparticles on the surface of activated carbon led to a lower surface area but, the magnetic property of MAC facilitated the separation of solid phase from aqueous solution much easier than AC.

© 2012 Published by Elsevier B.V.

1. Introduction

There has been growing concern for public health and environmental safety over the last few decades. Chemical pollution of surface water exhibits a threat to the aquatic environment with hazardous effects [1,2]. P-nitrophenol (PNP) is an important chemical intermediate, serving as precursors of pharmaceuticals and pesticides [3]. The other sources for PNP are diesel fuel and gasoline exhaust which enter PNP into environment [3,4]. There are many methods to remove phenolic compounds from wastewater stream such as advance oxidation process (AOPs) [5–7] sonolysis [8–11] extraction [12], and adsorption [13–16]. Among these techniques, adsorption is widely used which is due to easy operation, simple design, and generation [17,18]. Adsorption processes with biological materials, mineral oxides, activated carbons, or polymer resins have attracted attention [19]. Production of low cost AC from natural material is an important case. A number of paper report chemical and thermal treatment of agricultural by-product as precursors for the preparation of carbon-based adsorbents [20–23]. Chemical treatment on agricultural waste affects on the surface properties of AC and introduces some functional groups on the surface [24]. The adsorption of PNP onto AC was found to mainly depend on porosity and surface chemistry of carbons. AC with micropore size in the range of 0.74–2.21 nm strongly influenced

* Corresponding author. Tel./fax: +98 511 8795457.
E-mail address: moh_entezari@yahoo.com (M.H. Entezari).

1385-8947/$ - see front matter © 2012 Published by Elsevier B.V.
http://dx.doi.org/10.1016/j.cej.2012.08.011

the adsorption capacity [25]. The surface characteristics of AC depend on the content of heteroatoms such as oxygen or nitrogen which determine the charge, hydrophobicity, and electronic density of the graphene layers. Other crucial parameters are related to the properties of adsorbate molecules, molecular size, solubility, p*K*a, character of functional group attached on the aromatic rings [26]. In addition, the adsorptive capacity of granular AC for phenolic compounds may increase up to 3-fold in the presence of molecular oxygen. The cocoa shell based AC was used for the removal of PNP [25]. It was found that the main mechanism is chemisorptions based on π–π dispersive interaction. Also, the other agricultural wastes such as apricot stone [1], waste coke [27], sawdust [28] were used for the removal of phenolic compound from aqueous medium.

One of the promising methods for the removal of contaminants is the combination of sorption process and ultrasonic irradiation. There are many works in the literature about the use of ultrasonic irradiation for the removal of pollutants such as heavy metals [15,16], dyes [29,30], and phenolic compounds [31]. Ultrasound has been proven to be a very useful tool to enhance the mass transfer and in some cases to break the affinity between sorbate and sorbent. It was found that the adsorption rate of phenol onto activated carbon and Dowex resin in mixing method with 250 rpm was higher than ultrasonic irradiation at frequency of 1 MHz and 60 W [32]. Similar behavior was found by Wang and Cheng [33]. In the latter case the uptake of 4-(2-pyridylazo) resorcinol (PAR) onto Amberlite XAD-2 resin showed higher effect with stirrer method than 20 kHz ultrasonic irradiation. In comparison, Hamdaoui and Naffrechoux [31] investigated the adsorption of p-chlorophenol onto activated carbon. They found that the adsorption rate, the adsorbed amount, and the diffusion rate improved in the presence of ultrasonic irradiation with different frequencies.

In these kinds of removal, the problem is the separation of sorbent like AC from aqueous solution. Magnetic filtration is emerging as a water treatment technology which can provide rapid, efficient removal from wastewater stream [19,34]. After sorption process, the sorbent could be easily separated from solution using a magnetic separator. Different magnetic sorbents were reported such as magnetic ion exchange resins, magnetic zeolites, magnetic chitosan beads, magnetic silica with core shell structure, and magnetic nanoparticles impregnated agricultural wastes [35–39]. There are some reports about the magnetic AC in the literature [19,40–46].

In order to obtain a novel nanocomposite, carrot dross was recycled into a low cost AC and converted into magnetic AC. Then both samples (magnetic and nonmagnetic) were used for the PNP removal from aqueous solution.

2. Experimental

2.1. Chemical and equipment

Iron(III) chloride·6H_2O, iron(II) chloride·4H_2O, ammonia solution (25%), NaOH, HNO_3, HCl, and p-nitrophenol were purchased from Merck. NaCl and $NaHCO_3$ were purchased from Riedel-de-Haen Company. Na_2CO_3 was purchased from Fluka. Milli-Q water was used with a resistivity not less than 18.2 MΩ cm^{-1}.

The sorption processes in the presence of ultrasonic irradiation were carried out with Sonics and Material, 750 W, 20 kHz. Ultrasonic irradiations were performed in a water-jacketed rosette-cell with internal diameter 6 cm and height 11 cm. The 20 kHz wave was emitted by titanium probe (diameter 1.1 cm) and power supply VCX 750 W, with piezoelectric lead zirconate titanate crystal (PZT). The ultrasonic intensity of sonicator was measured through calorimetric method [51,52] and it was 17 W cm^{-2}.

2.2. Preparation of AC

The carrot dross was collected from local fruit juice factory. It was dried on the heater and washed with milli-Q water to remove impurity like dust, and then dried in oven at 100 °C overnight and finally grinded. Then, the powder was treated by diluted nitric acid to extract soluble organic compounds and introduce functional groups onto the surface of raw material. After that the powder was filtered, washed with milli-Q water several times and dried. Finally, the treated material was carbonized at 500 °C under air atmosphere for 1 h. Once the final temperature was reached, the furnace switched off. The as prepared sample was used for magnetization and adsorption processes.

2.3. Preparation of MAC

The magnetite nanoparticles were synthesized by modified Yanhui Ao method [45]. The procedure for the synthesis was as follows: definite amount of iron(III) chloride and iron(II) chloride with mole ratio of Fe(II)/Fe(III) equal to 1/2 were dissolved in 50 mL of milli-Q water and poured into a three necked balloon and bubbled with Ar for 15 min. Then ammonia solution (25%) was added drop-wise into the solution under vigorous stirring till the pH of the solution reached to 9.0. Finally, the black magnetite sol was obtained. The MAC was prepared as follows too: the obtained magnetite sol was diluted to 350 mL by addition of milli-Q water. Then 4 g of AC powder was added into diluted magnetic sol. The mixture was stirred for 1 h in the Ar atmosphere (Scheme S1). Finally, the solid phase was separated by a magnet and then dried at room temperature.

2.4. Physical and chemical characterization

The porous structure of the synthesized sorbents was studied by N_2 adsorption at 77 K using Quantachrome surface area analyzer (model Autosorb-1). Prior to the analysis, the sample was out-gassed at 100 °C for 12 h to a residual pressure of 10^{-4} torr or less. The surface area and pore size distribution were determined using Brunauer Emmett Teller (BET) equation [47]. To investigate the surface properties, the Fourier transform infrared (FTIR) for all samples recorded between 400 and 4000 cm^{-1} using Thermo Nicolet, Avatar 370 FTIR. The surface morphology of AC and MAC was examined using scanning electron microscopy (SEM) model Hitachi S-4160. The X-ray diffraction (XRD) of the product was recorded by Bruker, D8ADVANCE, Germany (X-ray Tube Anode: Cu, Wavelength: 1.5406 Å (Cu Kα) Filter: Ni). The XRD was used to identify the crystal structure and the average size of the nanoparticles. The average crystallite size was calculated by Debye–Sherrer's equation [48]. The magnetic property of the magnetite nanoparticle and magnetic AC was investigated using vibrating sample magnetometer (VSM), Leckeshore model.

2.5. Zero point charge measurement (pH_{pzc})

The pH_{pzc} of AC and MAC were determined experimentally [19,49]. The pH_{pzc} was measured using 0.01 M NaCl aqueous solutions at pH 2, 4, 6, 8, and 10. These pH values were fixed with HCl and NaOH aqueous solution. Each prepared solutions (10 mL) were contacted with 0.02 g of sample and the system was stirred for 48 h. The supernatant was decanted and its pH was measured. The pH_{pzc} value was determined from a plot of pH of the filtered solution (pH_f) as a function of initial pH value (pH_i) solutions [1,50].

2.6. Oxygen functional groups

The oxygen-containing functional groups for both samples AC and MAC were determined by applying the Boehm test with bases $NaHCO_3$, $NaCO_3$, and NaOH and also HCl as an acid reagent. About 0.5 g sample was contacted with 50 mL of 0.05 M base or acid solution in sealed flasks. The suspension was stirred for 24 h and then filtered. Then 10 mL of each solution was pipetted to a flask and titrated with 0.05 N sodium hydroxide and/or hydrochloric acid, depending on the original solution used. According to the Boehm test, the free carboxyl groups are neutralized with $NaHCO_3$, carboxylic groups and carboxyl groups in lacton-like binding structure can neutralize with Na_2CO_3, and phenolic hydroxyl groups on the surface of carbon along with carboxylic and lactonic groups react with NaOH solution. The reaction between reagents and acidic oxygenated-functional groups on the surface is based on the difference in acid/base strength [1,50].

2.7. Liquid phase adsorption

The adsorbate in liquid-phase was PNP with molar mass of 139.11 g mol^{-1}, water solubility of 161 g L^{-1} at 298 K and p*K*a = 7.13. The kinetic studies of the adsorption of PNP in a batch system were carried out at 24 ± 1 °C with pH = 4.0 ± 0.5. The temperature was held constant during the sonochemical and conventional processes by a water jacket in a rosette cell and a dual wall cell, respectively.

In these experiments, a certain amount of adsorbent (AC or MAC) was transferred to the reactor containing 50 mL of PNP aqueous solution at different initial known concentrations. The adsorption isotherms were determined for 0.1 g of AC or MAC with different initial concentrations (50–500 mg L^{-1}) of the pollutant at the optimum time to reach equilibrium condition. The kinetic studies of the adsorption of PNP in a batch system were carried out at 25 ± 1 °C with pH = 4.0 in the presence and absence of ultrasonic irradiation. In these experiments, a certain amount of adsorbent (AC or MAC) was transferred to the ultrasonic reactor containing 50 mL of PNP aqueous solution at different initial known concentrations. Ultrasonic waves at intensity of 17 W cm^{-2} as measured by calorimetric method were used for sonication. Then the results obtained under ultrasound were compared with the results of stirring method. The residual concentration of the pollutant was determined by UV–vis spectroscopy (Unico 2800) in acidic form at maximum absorbing wavelength (λ = 315 nm). The amount of PNP was measured in appropriate pH that ensured only the presence of one of the forms of the compound.

The adsorption of pollutant per unit gram of adsorbent, q_e, was evaluated from the following equation:

$$q_e = \frac{V(C_0 - C_e)}{M} \quad (1)$$

where V is the volume of solution, C_0 is the initial concentration of the adsorbate in solution, C_e is the concentration of solute in the bulk phase at equilibrium and M is the mass of the adsorbent.

In the case of pH study, the initial pH was adjusted by HCl and NaOH solutions. The pH was measured using pH-meter (metrohm 827).

One experiment was also run in the presence of ultrasonic irradiation without any sorbents (AC and MAC) and the other conditions were the same as experiment under sonication to determine the effect of ultrasonic irradiation alone on the degradation of PNP.

3. Results and discussion

3.1. Characterization of AC and MAC

3.1.1. Structure and morphology

Based on the XRD pattern of magnetite nanoparticles, the XRD peaks can be indexed to the (220), (311), (400), (511), and (440) for the face center cubic magnetite (Fe_3O_4) structure in accordance with JCPDS card of Fe_3O_4 (JCPDS-19-0629). The lattice parameter a = 8.361(02) Å and $V(a^3)$ = 69.906655(4404) (Å^3). (Fig. S1. Supporting information). In the case of MAC (Supplementary data, Fig. S1b), the pattern shows one peak centered at about $2\theta = 24°$ which corresponds to the (002) reflexes of crystalline graphite and also confirms the presence of magnetite nanoparticles in MAC sample. The mean size of the single crystallite can also be determined from the full-width at half-maximum of corresponding X-ray diffraction peaks by using Scherrer's formula $D = \frac{k\lambda}{\beta \cos\theta}$ [53], where λ is the wavelength of the X-ray radiation, k is the Scherrer constant (k = 0.9), θ is the characteristic X-ray radiation and β is the full-width at half maximum of the peaks. The estimated nanocrystallite size of Fe_3O_4 sample was 11.7 nm.

The SEM micrographs of AC and MAC with two mass ratios of Fe_3O_4/AC equal to 1/8 and 1/5 are shown in Fig. 1. A porous spongy texture in the case of AC can be shown in Fig. 1a and b. The micrographs in Fig. 1c–f show the morphological changes due to iron oxide impregnation on the surface of carbon matrix with mass ratios of 1/8 and 1/5, respectively. After iron oxide impregnation, the surface texture shows more spongy structure especially in ratio 1/5 than AC. It is suggested that the formation of well-dispersed iron oxide nanoparticles covering AC led to such structure. Also, the surface of carbon matrix shows more defects after impregnation.

3.1.2. Magnetic properties

The graph of magnetization versus applied magnetic field at room temperature was shown in Fig. 2 for Fe_3O_4 and MAC in two different ratios (Fe_3O_4/AC, 1/8 and 1/5).

According to the results, the magnetic parameters such as saturation magnetization (Ms) for iron oxide, MAC (1/5) and MAC (1/8) were 70, 2.22, and 1.22 $emug^{-1}$, respectively. Both samples present the superparamagnetic behavior. Therefore, they can be separated easily in a suspended system. Moreover, the particles can be re-dispersed after they are separated by an external magnetic field which is due to its superparamagnetic behavior. In MAC, the magnetic saturation decreases for both mass ratios. This is attributed to the low contribution of the mass of the nonmagnetic particles to the total sample mass. The inset of Fig. 2 shows the illustration about magnetic separation of sample 1:8 with 0.4 T magnet. The separation was occurred in 7 min.

3.1.3. Surface measurements

The plots of pore volume versus pore diameter show that both AC and MAC possess mainly micropores structures (Fig. S2. Supporting information). Furthermore, there are no significant differences between AC and MAC in view of porosity structure and pores diameter. The total pore volume (V_T) for AC and MAC (1/8) is 0.24 $cm^3\ g^{-1}$ and for MAC (1/5) is 0.18 $cm^3\ g^{-1}$. The N_2 adsorption–desorption isotherms of AC and MAC (1/8 and 1/5) in Fig. 3 present the isotherm of type (I) with denoting micropore solid [19,54], but the isotherm shows a hysteresis of H4 type [55]. Actually, the type H4 loop is often associated with narrow slit-like pores, but in this case the type (I) isotherm character is indicative of microporosity [55].

The relative high microporosity of the carbon from carrot dross can be partly attributed to the higher cellulose content of the raw materials [1].

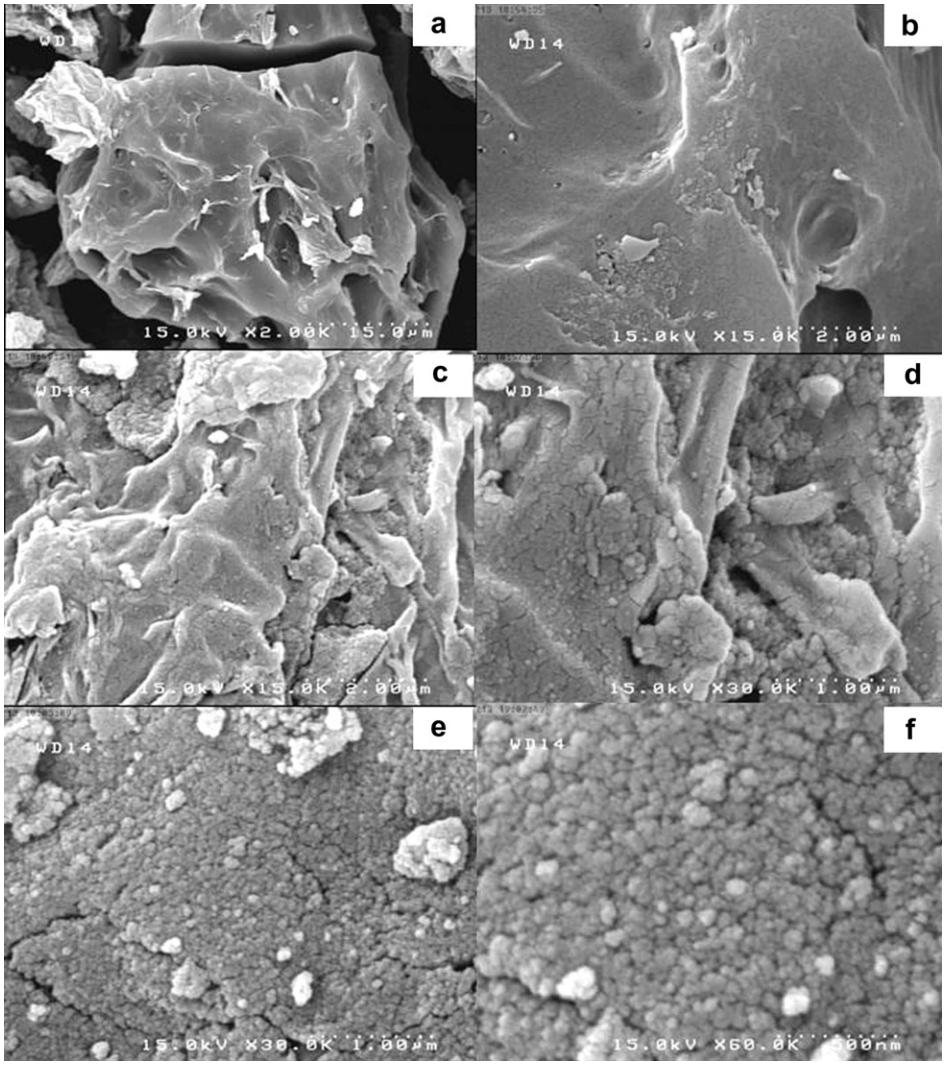

Fig. 1. (a and b) SEM micrograph of AC, (c and d) MAC with Fe_3O_4/AC mass ratio of 1:8, and (e and f) MAC with Fe_3O_4/AC mass ratio of 1:5.

Microporosity volume is smaller for MAC (1/5) than the two other samples. Based on Table 1, surface area measurement (S_{BET}) and W_0 (micropore volume, Dubinin–Radushkevich equation) are 447 $m^2\ g^{-1}$ and 0.23 $cm^3\ g^{-1}$ for AC, 435 $m^2\ g^{-1}$ and 0.22 $cm^3\ g^{-1}$ for MAC (1/8), 340 $m^2\ g^{-1}$ and 0.17 $cm^3\ g^{-1}$ for MAC (1/5), respectively. The smaller surface area and pore volume of MAC samples can be attributed to the covering of AC surface by iron oxide nanoparticles which confirmed by the SEM results. Therefore, the study was focused on the MAC with ratio 1/8 which has a higher surface area with magnetic properties.

3.1.4. Surface functional groups

The identification and quantification of the oxygen groups of AC and MAC (1/8) is shown in Table 2. According to the Boehm test, the amount of acidic groups (carboxylic, lactonic, and phenolic hydroxyl groups) was higher than basic groups. This should be related to the treatment of the sample by nitric acid which led to the acidic groups on the surface. It is seen that the order of the amount of acidic and basic groups for AC and MAC (1/8) are as follows:

AC: phenolic hydroxyl > **carboxyl** > **lactonic** > basic groups.
MAC: phenolic hydroxyl > **lactonic** > **carboxyl** > basic groups.

It is suggested that the interaction of Fe_3O_4 nanoparticles with the surface of AC led to reduction of functional groups. Furthermore, the amount of lactonic groups was higher than carboxylic groups for the MAC. It is assumed that during the impregnation process in alkali media, the carbonyl groups which are in close neighborhood of hydroxyl and carbonyl groups condense to lacton groups [50].

3.1.5. Point of zero charge (pH_{pzc})

The pH_{pzc} value for AC and MAC (1/8) are given in Table 3. The pH_{pzc} is defined as the pH where the net surface charge is zero. The higher the surface acidity led to lower pH_{pzc}. AC shows basic or acidic pH value in aqueous dispersion. A good correlation has been found between pH and oxygen content of the AC. The higher content of oxygen groups led to more acidic properties of the surface. They showed acidic and hydrophilic properties and adsorbed bases [50]. The pH_{pzc} was 2.2 for AC and 6.1 for MAC (1/8). The Boehm test confirms this result and shows more oxygen functional groups in the case of AC. Surface functional groups may cover a small fraction of the AC surface, but significantly influence the adsorption properties and reactivity of the AC.

3.1.6. Infrared spectroscopy analysis

The FTIR spectroscopy analysis was used to obtain information about the characteristic of sorbent and the interactions of sorbent–sorbate. To study the nature of sorbent, the FTIR spectrum of Fe_3O_4 nanoparticles, AC and MAC are shown in Fig. 4. The AC shows some

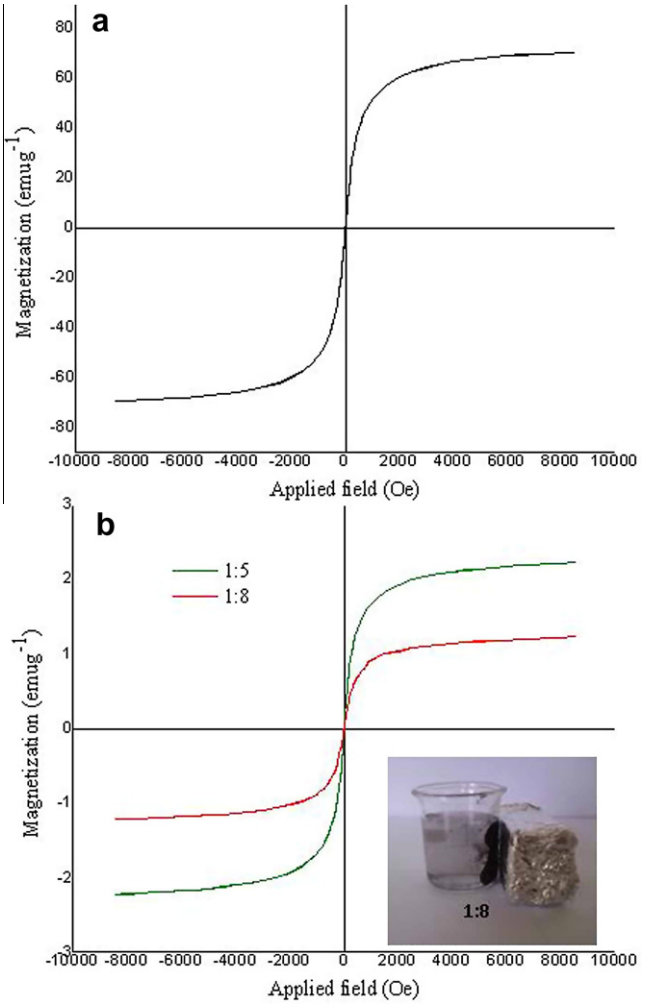

Fig. 2. Magnetization versus applied magnetic field for (a) magnetite nanoparticles and (b) MAC with Fe_3O_4/AC mass ratios of 1:5 and 1:8.

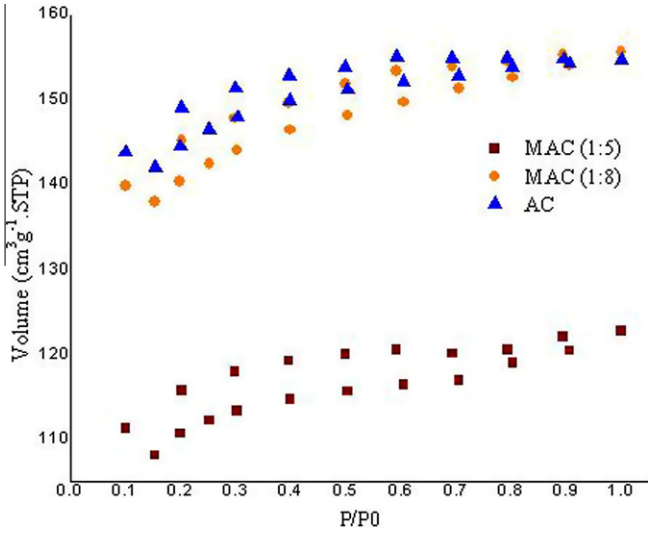

Fig. 3. BET isotherm plot of AC and MAC with mass ratios of 1:5 and 1:8.

peaks around 3440, 2960, 1620 with a small shoulder at 1760, 1250, and 1120 cm^{-1} due to *v* OH, C–H, C=O, and C–O groups, respectively. The peaks at 1620 and 1760 cm^{-1} assigned to carbonyl groups. In the case of MAC, the broad peak at 3440, and 1580 cm^{-1} related to *v* (O–H) and C=O. Also, a broad peak centered at 1223 cm^{-1} is seen. It is suggested that the coating of magnetite nanoparticles on the surface of AC led to this peak. This broad peak is obtained from combination of peaks which exist in this region. Also, the FTIR spectrum of Fe_3O_4 nanoparticles shows a peak at 552 cm^{-1} due to M–O band. Thus, the small peak at 570 cm^{-1} in MAC spectrum could be assigned to the iron oxide (Fe_3O_4) nanoparticles on the surface.

The spectrums of pure PNP, AC and MAC after sorption process in the presence and absence of ultrasonic irradiation were obtained to study the nature of sorbent–sorbate interaction (Fig. S3a–c). The O–H bond appears at 3440 cm^{-1} and shifted to lower frequency in both cases (sono-sorption and conventional methods). In the case of PNP, it is seen a double bond at 1620 cm^{-1} and 1600 cm^{-1} and a bond at 1510 cm^{-1} due to C=C bond of phenyl group which shifted to lower frequency at 1610 cm^{-1} with a shoulder at 1590 cm^{-1} and a peak around 1418 cm^{-1} (red shift, increased wavelength) are due to phenyl group of adsorbed PNP on the surface of AC (after sono-sorption). The adsorption of PNP on the surface of AC led to weaker binding in PNP and red shift. Furthermore, the peaks at 1350, 1290, 1220, and 1170 cm^{-1} in pure PNP shifted to 1290, 1240, 1190, and 1120 cm^{-1} attributed to adsorption of phenyl groups and N=O group on the surface of AC.

In the case of adsorption process using stirrer method, AC shows a broad peak around 600–1585 cm^{-1} due to combination of peaks at this region. This broad peak confirms the adsorption of PNP on the surface of carbon active. But, the interaction of sorbent–sorbate is significantly different in stirring than ultrasonic method. It is suggested that the adsorption process without ultrasonic irradiation might be multilayer or there are different adsorption sites with different energies. But, ultrasonic irradiation led to a monolayer adsorption with uniform adsorption sites.

Table 1
Surface area measurements of the AC and MAC with mass ratio of 1:5 and 1:8.

Samples	S_{BET} ($m^2\ g^{-1}$)	W_0 ($cm^3\ g^{-1}$)	V_T ($cm^3\ g^{-1}$)	Average pore diameter (Å)
AC	447	0.23	0.24	21.41
MAC (1:8)	435	0.22	0.24	22.10
MAC (1:5)	340	0.17	0.18	22.33

S_{BET} (specific surface area, BET equation), W_0 (micropore volume, Dubinin–Radushkevich equation), V_T (total pore volume).

Table 2
Quantification of oxygen groups on AC and MAC surface (mmol g^{-1}).

Samples	Carboxyl	Lactonic	Hydroxyl phenolic	Total acidic groups	Total basic groups
AC	0.604	0.499	0.712	1.815	0.192
MAC (1:8)	0.252	0.389	0.707	1.348	0.143

Table 3
Determination of point of zero charge (pH_{pzc}) for AC and MAC (1:8).

AC		MAC (1:8)	
$pH_{(initial)}$	$pH_{(final)}$	$pH_{(initial)}$	$pH_{(final)}$
2.15	2.20*	2.15	2.35
4.15	2.20	4.15	5.11
5.63	2.66	5.63	6.10*
8.66	2.38	8.66	6.77
10.10	6.94	10.10	7.36

* Point of zero charge.

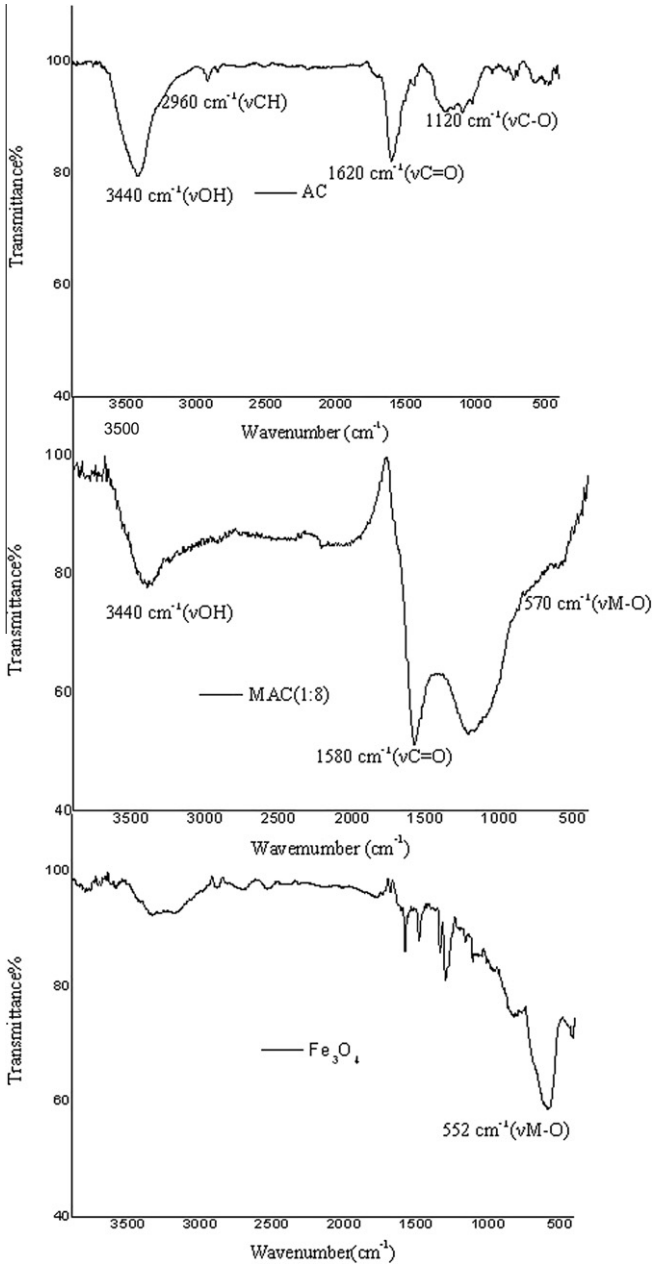

Fig. 4. FTIR spectrums of Fe_3O_4 nanoparticles, AC and MAC (1:8).

The FTIR spectrum of MAC after adsorption in the presence and absence of ultrasonic irradiation shows in Fig. S3c. As it is seen, the interaction of sorbent–sorbate is not significantly different between ultrasonic and conventional method. The O–H bond at 3400 cm^{-1} in MAC shifted to 3433, and 3423 cm^{-1} after sorption process by ultrasonic irradiation and conventional method, respectively. In addition, the center of broad peaks at 1580 and 1223 cm^{-1} shifted to 1590 and 1210 cm^{-1} for ultrasonic method and 1570 and 1150 cm^{-1} in the case of stirrer method. The red shifts especially in the case of stirrer method confirms the strong adsorption between PNP and MAC surface which led to weaker binding in PNP molecules and red shift.

3.2. Sorption study

3.2.1. Effect of initial pH

The effect of initial pH was studied on the adsorption of PNP onto AC and MAC (1/8) in the presence and absence of ultrasonic irradiation (Fig. 5 and Table S1. Supporting information). The pH of the solution is one of the crucial parameters influencing the adsorption capacity of sorbates such as phenolic compounds. To evaluate the effect of pH on the PNP sorption in 10 min, different experiments were conducted at 24 ± 1 °C in the pH range of 1.92–9.60 using 0.2 g of AC or MAC (1/8) with 50 mL of 50 mg L^{-1} adsorbate solution. The pH of medium affects the solubility of PNP as well as the ionization state of functional groups on the surface of AC and MAC. The PNP is a water-soluble solid that is moderately acidic in water (p*K*a = 7.15). When pH of the solution is lower than pH_{pzc}, the surface of AC or MAC is positive and the surfaces are negative when the pH is higher than pH_{pzc}. The pH_{pzc} for AC and MAC is 2.22 and 6.10, respectively and the PNP is in the molecular form when the pH is less than its p*K*a. At higher pH, the PNP molecules gradually ionized into PNP anions. According to the Fig. 5, the removal efficiency is more than 98% in the applied range of pH except at pH > 8.0 where the MAC and AC show marginally decrease in the presence and absence of ultrasonic irradiation. It is claimed that the adsorption capacity of phenolic compounds can be significantly decreased in alkali media and in pH > pH_{pzc}. It was found that under this condition the net charge of AC is negative and the PNP molecules are as anion form. Therefore, the electrostatic repulsion played an important role in the interaction between the surface of AC and PNP anions [1,56].

Fortunately, the final pH of solution in our case after 10 min decreased to acidic pH (Table S1). Therefore, the most of PNP molecules present in molecular structure forms and the repulsion is not predominant. This behavior is due to the surface properties of the synthesized sorbent. As it was mentioned before, the oxygen

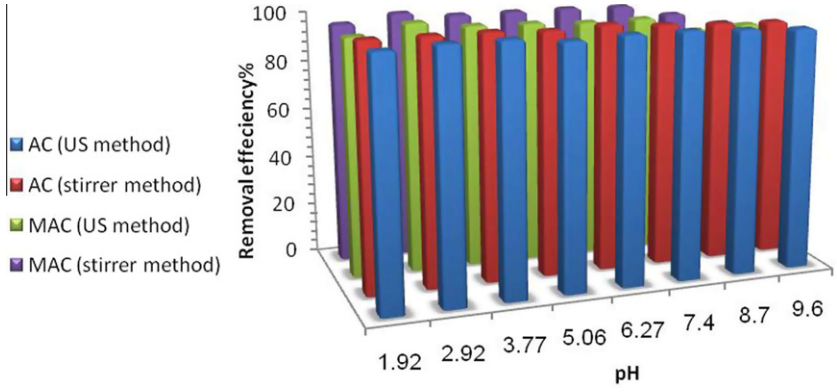

Fig. 5. Effect of initial pH on the sorption of PNP using AC and MAC (1:8) in the presence and absence of ultrasonic irradiation (time = 10 min, initial concentration = 50 mg L^{-1}, mass of sorbent = 0.2 g, t = 24 ± 1 °C).

containing groups on the surface of AC led to hydrophilic sites and acidic properties of the surface. The acidic properties of the AC surface decrease the pH of solution during the adsorption process and the electrostatic interaction between protonated functional groups of carbon surface and sorbate led to high removal efficiency in all pH range.

3.2.2. Effect of contact time and mass of sorbent

Fig. 6 shows the effect of contact time on the removal of PNP at two different masses of AC and MAC (0.1 and 0.2 g) over a time of 3–20 min by using 50 mL of 50 mg L^{-1} PNP at pH = 4.0 ± 0.5 and temp. 24 ± 1 °C in the presence and absence of ultrasonic irradiation. The removal efficiencies were 98%, 96.26%, 96.10%, and 96% for the AC under ultrasonic irradiation and stirrer method and MAC at these conditions, respectively (3 min and 0.2 g of sorbent). The rapid increase of removal efficiency in the initial stages indicated that there are plenty of readily accessible sites. Adsorption rate of PNP on AC and MAC was found to be relatively much faster than the other sorbents. The rate of adsorption was marginally higher in the presence of ultrasound for AC at low concentration of pollutant but, at higher concentrations (Fig. 7), the rate of removal was much higher in the presence of ultrasound. This means that, the sorbent has high available sorbent sites. At low concentrations of pollutant, there is a marginal different between the sorption in the presence and absence of ultrasound. By increasing the concentration of the pollutant the availability of the adsorption sites reduces and in this situation ultrasound has a positive effect

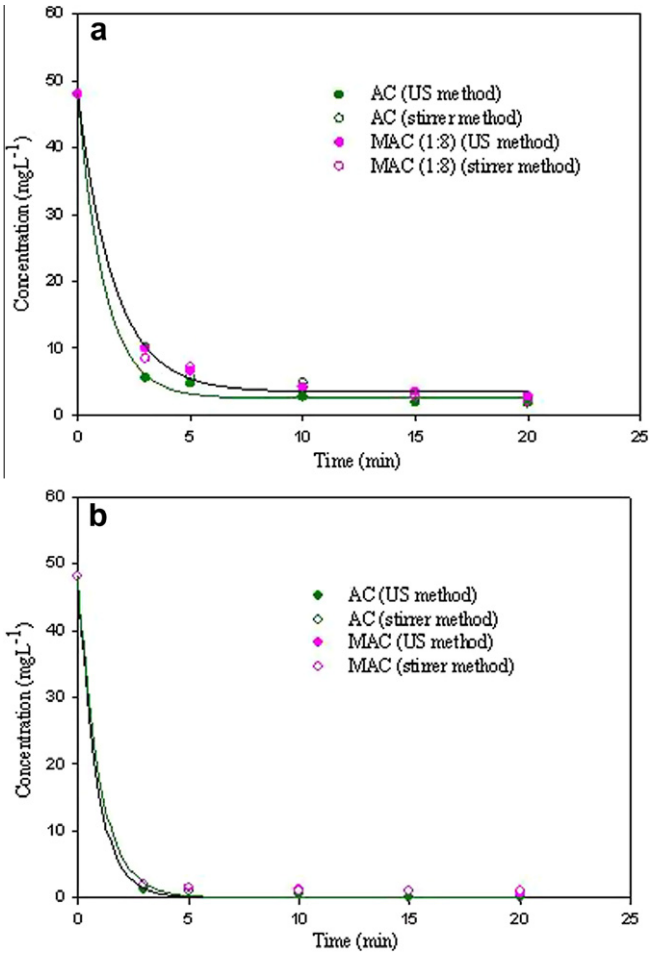

Fig. 6. Effect of contact time and mass of sorbent for the removal of PNP using AC and MAC (1:8) in the presence and absence of ultrasonic irradiation (a) 0.1 g, and (b) 0.2 g of sorbents (pH = 4.0 ± 0.5, t = 24 ± 1 °C).

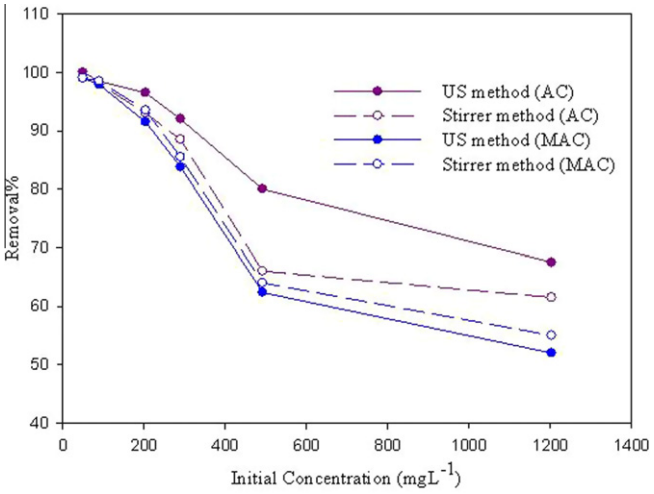

Fig. 7. Effect of initial concentration for the removal of PNP by AC and MAC (1:8) in the presence and absence of ultrasonic irradiation (pH = 4.0 ± 0.5, t = 24 ± 1 °C, mass of sorbent = 0.2 g, time = 20 min).

on the adsorption. In the case of MAC, the behavior is reversed and this might be related to the lower interaction of pollutant and the surface due to the presence of magnetic nanoparticles on the AC. With lower interaction, ultrasound can facilitate the desorption process. In heterogeneous system, the bubbles collapse asymmetrically and producing a high-speed jet of liquid, which passes through the interior of the cavitation bubble and toward the solid surface, called a microjet [57,58]. It has been reported that the speed of the liquid jet may reach to more than 100 m s^{-1} [57]. This type of microjet is responsible for erosion of the solid surface and particle breakage [31]. Therefore, the accessible surface sites increased and led to higher adsorption rate especially at higher concentrations of pollutant for AC. In the case of MAC, the surface of activated carbon was changed by coating of magnetite nanoparticles. Some accessible sites were covered by Fe_3O_4 nanoparticles and sorption rate decreased.

To determine the effect of ultrasonic irradiation on the degradation of PNP, one experiment was run without any sorbent (AC and MAC) under ultrasound. According to the results there was no degradation after 1 h soniation.

3.2.3. Effect of initial concentration

Fig. 7 presents the removal of PNP at various initial concentrations (50–1200 mg L^{-1}) in 20 min using 0.2 g of sorbent (AC or MAC) at pH = 4.0 ± 0.5 and temp 24 ± 1 °C in the presence and absence of ultrasonic irradiation. The results show that the removal efficiency decreased by increasing the initial concentration. The high removal efficiency in the applied range of concentrations in a short time confirms the presence of plenty accessible active sites on the surface of sorbent. Maximum adsorption capacity and removal efficiency were found for the AC in the presence of ultrasonic irradiation at high concentrations of the pollutant but not at low concentration. The higher adsorption rate by sonication might be attributed to the extreme conditions generated during the violent collapse of the cavitation bubbles. The asymmetric collapse of bubbles in a heterogeneous system produces micro-jets with high velocity. Furthermore, collapses generate shockwaves, which cause extremely turbulent flow at the liquid–solid interface, increasing the rate of mass transfer near the solid surface.

3.2.4. Adsorption isotherm model

As PNP molecules were mostly accommodated onto micropores [2], hence the lower micropore volume in the case of MAC (Table 1)

Table 4
Isotherm parameters of Langmuir and Freundlich model for the adsorption of PNP onto AC and MAC (1:8) in the presence and absence of ultrasonic irradiation.

Sample	Langmuir model				Freundlich model		
	q_m (mg g^{-1})	b (L mg^{-1})	R^2	R_L	K_F	n	R^2
AC (US method)	125	0.22	0.99	0.0090	26.66	3.52	0.91
AC (stirrer method)	91	0.19	0.95	0.0104	22.43	3.43	0.98
MAC (US method)	84	0.12	0.98	0.0163	17.7	2.82	0.99
MAC (stirrer method)	85	0.18	0.96	0.0109	20.32	3.33	0.98

can cause a decrease of adsorption capacity (Fig. S4). These results indicate that the sorption process dependent upon surface are, porosity, and possibility the surface functional groups.

The results were analyzed with the well-known models of Langmuir and Freundlich. The linear form of Langmuir isotherm is given by the following equation:

$$\frac{1}{q_e} = \frac{1}{q_m} + \frac{1}{bq_mC_e} \quad (2)$$

where C_e (mg L^{-1}) is the equilibrium concentration of the adsorbate, q_e (mg g^{-1}) is the amount of adsorbed per unit mass of adsorbent, q_m (mg g^{-1}) and b are Langmuir constants.

The linear form of Fruendlich isotherm is:

$$\log q_e = \log K_F + \frac{1}{n}\log C_e \quad (3)$$

where K_F is roughly an indicator of the adsorption capacity and ($1/n$) of the adsorption intensity. Value of $n > 1$ represent a favorable adsorption condition [28]. The data about the Langmuir and Freundlich isotherms are given in Table 4.

Furthermore, the Freundlich constant is lower in the case of PNP adsorption onto MAC in the presence of ultrasonic irradiation which indicate that the low adsorption capacity.

As shown in Table 4, the data for adsorption of PNP onto AC under ultrasonic irradiation was well fitted with Langmuir model but under the other conditions the data were not well fitted with Langmuir and consistent with Freundlich isotherm, indicating the surface energies is not uniform. Some of the sites were highly energetic and bound the adsorbed PNP strongly, whereas some were much less energetic and bound PNP weakly, which resulted in the possibility of more than just one monomolecular layer of coverage on the AC or MAC surfaces. Thus, the adsorption of PNP in multimolecular layers was indicated in view of experimental data. The uniform and monomolecular adsorption on the AC under ultrasonic irradiation was due to the extreme conditions generated during the violent collapse of cavitation bubbles. The asymmetric collapse of bubbles in a heterogeneous system produces micro-jets with high velocity led to uniform energy distribution of adsorption sites on the surface of AC. In the case of MAC in the presence of ultrasonic irradiation, the isotherm was fitted with both Langmuir and Freundlich isotherms but fitted better with Freundlich model. The presence of iron oxide on the surface of carbon active causes different energy sites on the surface. The FTIR results confirm the differences between adsorption on the surface of AC. Under ultrasonic irradiation a monomolecular layer of adsorption and in the absence of ultrasonic irradiation a multimolecular adsorption or different adsorption sites can be observed.

3.2.5. Adsorption kinetic models

The experiments were conducted with 50 mL solution (50 mg L^{-1}) at 24 ± 1 °C, pH = 4.0 ± 0.5, and 0.1 g of sorbent. To analyze the adsorption kinetic models, Lagergren's pseudo-first order and McKay and Ho's pseudo-second order [59,60] models were applied to the experiment data and the experimental results well-defined to pseudo-second order equation.

Table 5
Kinetic parameters for the adsorption of PNP onto AC and MAC (1:8) in the presence and absence of ultrasonic irradiation.

Sample	Pseudo-second order			
	k_2 (g(mg min)$^{-1}$)	$q_{e,cal}$ (mg g^{-1})	R^2	$q_{e,exp}$ (mg g^{-1})
AC (US method)	0.180	23.40	0.9999	26
AC (stirrer method)	0.125	22.87	0.9999	24.37
MAC (US method)	0.124	22.80	0.9999	23.50
MAC (stirrer method)	0.140	23.10	0.9999	24

The pseudo-second order equation expressed as;

$$\frac{t}{q_t} = \frac{1}{k_2q_e^2} + \frac{t}{q_e} \quad (4)$$

where k_2 is the rate constant of second order adsorption. The slope and intercept of plots of $\frac{t}{q_t}$ versus t (figures not shown) were used to calculate the second rate constant k_2. The pseudo-second order rate constant (k_2), correlation coefficients (R^2) along with the experimental and calculated uptake capacity (q_e) are presented in Table 5.

3.2.6. Adsorption mechanism

Adsorption is a multi-steps process involving transport of ingoing adsorbate to external surface of the adsorbent (film diffusion), transport of the adsorbate within the pores of the adsorbent, and adsorption of ingoing adsorbate on the interior surface of the adsorbent [56]. The adsorption processes may be controlled either by one or more steps. The intraparticle diffusion rate equation is given by [61]:

$$q_t = k_it^{0.5} + c \quad (5)$$

where k_i is the intraparticle diffusion rate constant and c is the intercept. The k_i value can be calculated from the linear plots of q_t versus $t^{0.5}$. The values of c give information about the thickness of the boundary layer, i.e., the larger the intercept, the greater the boundary layer effect [25]. The multi-linearity of the plot indicating that more than one step influences the sorption process (Fig. S5. Supporting information). It is assumed that an external mass transfer followed by a gradual adsorption stage with intraparticle diffusion dominating. Based on Fig. S5 in Supplementary data, the plot of the amount of PNP adsorbed at time t versus the square root of time using AC and MAC (1:8) in the presence and absence of ultrasonic irradiation showed a rapid diffusion in the first stage. This can be attributed to the diffusion of PNP through the external surface of

Table 6
Intraparticle diffusion rate constants (k_i and c) and mode of diffusion parameters at different.

Sample	k_i (mg g^{-1} min$^{-0.5}$)	c	R^2	k_m	n
AC (US method)	1.218	18.52	0.98	0.770	0.0495
AC (stirrer method)	0.531	20.19	0.98	0.729	0.0856
MAC (US method)	0.472	20.43	0.99	0.752	0.086
MAC (stirrer method)	0.691	19.84	0.98	0.750	0.082

the sorbent. This was followed by intraparticle diffusion of PNP molecules to the sites on the surface. The intraparticle diffusion rate constants obtained from the slope of the second portion of Fig. S5 are shown in Table 6. Since the second portion of the curve did not pass through the origin, it is assumed that the intraparticle diffusion was not the only rate controlling step and that boundary layer diffusion controls the sorption process to some degree [53]. As Table 6, it is observed that the intraparticle diffusion rate is higher for the adsorption of PNP on the surface of AC in the presence of ultrasonic irradiation than conventional method. Furthermore, the value of c is lower for the AC (US method) than AC (stirrer method). Many studies have shown that boundary layer diffusion is dominant during the initial adsorbate uptake. Then, the adsorption rate gradually becomes controlled by intraparticle diffusion [31]. It is suggested that the higher value of diffusion rate constant and smaller value of c as thickness of boundary layer in the presence of ultrasound indicate that ultrasound enhances the mass transport in the pores and reduces the boundary layer thickness.

In the case of MAC (1:8), the diffusion rate constant (k_i) is lower and boundary layer thickness (c) is higher in the presence of ultrasonic irradiation. As discussed before, it is assumed that this behavior is related to the breaking of sorbent–sorbate affinity by ultrasonic irradiation. Since, presence of iron oxide changed the surface properties of activated carbon and led to higher boundary layer resistance.

To know the mode of diffusion, the transport number was computed from the following equation [62]:

$$\log \frac{q_t}{q_e} = \log k_m + n \log t \quad (6)$$

where k_m is the adsorbate–adsorbent interaction coefficient and n is the transport number. In order to calculate n and k_m, $\log \frac{q_t}{q_e}$ was plotted versus $\log t$. The values of k_m and n are shown in Table 6. The value of n indicates the type of transport mechanism. A value of $n = 0.5$ represent the Fickian mechanism and $n = 1$ indicates the non-Fickian mechanism. The constant k_m depends on the characteristic of the adsorbents in addition to its interaction with PNP molecules. The value of n was found to be less than 0.5 (Table 6), indicating the Fickian diffusion of PNP with the surface interaction of PNP molecules on the adsorbent surface.

In addition, the surface property of carbons strongly influences the adsorption of organic molecules from aqueous phase. The carbon surface properties are influenced to a large extent by the foreign elements fixed on the surface, in particular by oxygen. Several parameters have been proposed to contribute for the phenolic compound adsorption on the carbonaceous materials:

- Adsorbate molecular size and pore size of the adsorbent: the increase of adsorption is expected when the diameter of adsorbate molecule is twice smaller than the micropore size [23]. The size of PNP molecules is estimated to be 0.75 nm. In our case, AC and MAC with mean micropore size about 2.2 nm present suitable surfaces for the adsorption of PNP molecules.
- Type of interactions between carbonaceous materials and phenolic compounds: the adsorption mechanisms include (1) π–π dispersion interactions between AC basal planes and the phenolic ring, (2) electrostatic attraction and repulsion forces, (3) hydrogen-bonding between adsorbate and carbon surface functions, and (4) donor–acceptor complex formation. It seems that the main mechanism of interactions of sorbate molecular forms with carbon surface is the dispersion interactions between the π electrons of carbon graphene layers and solute aromatic ring. But, the treatment of carbonaceous materials with nitric acid produced oxygen functional groups on the surface of AC. These functional groups reduced the surface hydrophobicity and the electron density of graphene layers [24]. However, $-NO_2$ group on the PNP molecules has strongly electron-withdrawing properties which decreases the electron density and dispersive interaction. Therefore, the dominant interaction of PNP on the surface of AC and MAC should be the hydrogen bonding interactions between –COOH and –OH surface functions with the oxygen of nitro groups in PNP. In addition, the electrostatic interaction of polar surface groups with PNP should be considered.

4. Conclusion

AC and MAC were prepared, characterized and used successfully for the PNP remediation from aqueous media. The surface area obtained for AC was 447 $m^2 g^{-1}$ versus 435 and 340 $m^2 g^{-1}$ for MAC with different mass ratio of (1:8) and (1:5), respectively. Adsorption of PNP onto AC and MAC was carried out without and with assistance of ultrasound. Adsorption of PNP onto activated carbons does not significantly change with different initial pH solution. The adsorption capacity and removal efficiency reduced with increasing of magnetic nanoparticle content on the surface of activated carbon.

Two isotherm models, Freundlich and Langmuir, were tested for all samples. All of them were fit well by Freundlich model except adsorption of PNP molecules on the surface of AC under ultrasonic irradiation which fitted with Langmuir model. The PNP adsorption rate fits with pseudo-second order kinetic model where the rate-limiting step is assumed to be chemical sorption between the adsorbate and the adsorbent. Comparison of the data between ultrasonic and conventional method, both the adsorption rate and the adsorbed amount were significantly enhanced in the presence of ultrasonic irradiation for AC at high concentrations of pollutant. In the case of AC, the value of the intraparticle diffusion rate constant obtained in the presence of ultrasound was greater than those obtained in conventional method. Hydrodynamic effects induced by ultrasound promote a significant increase of the mass transfer across the boundary layer. The MAC particles can readily be recovered from the solution using permanent magnet. In addition, it is easily re-dispersed in the solution upon removing the magnetic field. This work improved an effective low cost MAC exhibiting a reasonably high surface area with high efficiency for the removal PNP compound. MAC was easily manipulated by a low strength external magnetic field and permitting an easy recovery from aqueous media.

Appendix A. Supplementary material

Supplementary data associated with this article can be found, in the online version, at http://dx.doi.org/10.1016/j.cej.2012.08.011.

References

[1] B. Petrova, T. Budinova, B. Tsyntsarski, V. Kochkodan, Z. Shkavro, N. Petrov, Removal of aromatic hydrocarbons from water by activated carbon from apricot stones, Chem. Eng. J. 165 (2010) 258–264.
[2] D. Tang, Z. Zheng, K. Lin, J. Luan, J. Zhang, Adsorption of p-nitrophenol from aqueous solutions onto activated carbon fiber, J. Hazard. Mater. 143 (2007) 49–56.
[3] Ö.S. Kuşçu, D.T. Sponza, Performance of anaerobic baffled reactor (ABR) treating synthetic wastewater containing p-nitrophenol, Enzyme Microb. Technol. 36 (2005) 888–895.
[4] J. Tremp, P. Mattrel, S. Fingler, W. Giger, Phenols and nitrophenols as tropospheric pollutants: emissions from automobile exhausts and phase transfer in the atmosphere, Water Air Soil Pollut. 68 (1993) 113–123.
[5] O. Gimeno, M. Carbajo, F.J. Beltran, F.J. Rivas, Phenol and substituted phenols AOPs remediation, J. Hazard. Mater. B 119 (2005) 99–108.
[6] M. Ksibi, A. Zemzemi, R. Boukchina, Photocatalytic degradability of substituted phenols over UV irradiated TiO_2, J. Photochem. Photobiol. A: Chem. 159 (2003) 61–70.

[7] P. Canizares, J. Lobato, R. Paz, M.A. Rodrigo, C. Saze, Electrochemical oxidation of phenolic wastes with boron-doped diamond anodes, Water Res. 39 (2005) 2687–2703.
[8] M.H. Entezari, C. Petrier, A combination of ultrasound and oxidative enzyme: sono-biodegradation of substituted phenols, Ultrason. Sonochem. 10 (2003) 241–246.
[9] M.H. Entezari, C. Petrier, A combination of ultrasound and oxidative enzyme: sono-enzyme degradation of phenols in a mixture, Ultrason. Sonochem. 12 (2005) 283–288.
[10] M.H. Entezari, M. Mostafai, A. Sarafraz-yazdi, A combination of ultrasound and a bio-catalyst: removal of 2-chlorophenol from aqueous solution, Ultrason. Sonochem. 13 (2006) 37–41.
[11] M.H. Entezari, A. Heshmati, A. Sarafraz-yazdi, A combination of ultrasound and inorganic catalyst: removal of 2-chlorophenol from aqueous solution, Ultrason. Sonochem. 12 (2005) 137–141.
[12] S.W. Peretti, C.J. Tompkins, J.L. Goodall, A.S. Michaels, Extraction of 4-nitrophenol from 1-octanol into aqueous solution in a hollow fiber liquid contactor, J. Membr. Sci. 195 (2001) 193–202.
[13] J. Rivera-Utrilla, M. Snchez-Poloa, V. G?mez-Serrano, P.M. Alvarez, M.C.M. Alvim-Ferraz, J.M. Dias, Activated carbon modifications to enhance its water treatment applications. An overview, J. Hazard. Mater. 187 (2011) 1–23.
[14] L.M. Cotoruelo, M.D. Marqués, F.J. Díaza, J. Rodríguez-Mirasol, J.J. Rodríguez, T. Cordero, Adsorbent ability of lignin-based activated carbons for the removal of p-nitrophenol from aqueous solutions, Chem. Eng. J. 184 (2012) 176–183.
[15] M.H. Entezari, T. Rohani Bastami, Sono-sorption as a new method for the removal of lead ion from aqueous solution, J. Hazard. Mater. B 137 (2006) 959–964.
[16] M.H. Entezari, T. Rohani Bastami, Influence of ultrasound on cadmium ion removal by sorption process, Ultrason. Sonochem. 15 (2008) 428–432.
[17] A. Bhatnagar, M. Sillanp, Utilization of agro-industrial and municipal waste materials as potential adsorbents for water treatment—a review, Chem. Eng. J. 168 (2010) 493–504.
[18] D. Sud, G. Mahajan, M.P. Kaur, Agricultural waste material as potential adsorbent for sequestering heavy metal ions from aqueous solutions – a review, Bioresour. Technol. 99 (2008) 6017–6027.
[19] M. Dinesh, S. Ankur, V.K. Singh, M. Alexandre-Franco, C.U. Pittman Jr., Development of magnetic activated carbon from almond shells for trinitrophenol removal from water, Chem. Eng. J. 172 (2011) 1111–1125.
[20] T.J. Bandosz, Activated Carbon Surface in Environmental Remediation, First ed., Interface Science and Technology Series; Elsevier, New York, 2006.
[21] D. Savova, E. Apak, E. Ekinci, F. Yardim, N. Petrov, T. Budinova, V. Minkova, Biomass conversion to carbon adsorbents and gas, Biomass Bioenergy 21 (2001) 133–142.
[22] N. Petrov, T. Budinova, M. Razvigorova, J. Parra, P. Galiatsatou, Conversion of olive wastes to volatiles and carbon adsorbents, Biomass Bioenergy 32 (2008) 1303–1310.
[23] T. Budinova, D. Savova, B. Tsyntsarski, C.O. Ania, B. Cabal, J.B. Parra, N. Petrov, Biomass waste-derived activated carbon for the removal of arsenic and manganese ions from aqueous solutions, Appl. Surf. Sci. 255 (2009) 4650–4657.
[24] I.P.P. Cansado, P.A.M. Mourão, A.I. Falcão, M.M.L. Ribeiro Carrott, P.J.M. Carrott, The influence of the activated carbon post-treatment on the phenolic compounds removal, Fuel Process. Technol. 103 (2012) 64–70.
[25] F. Ahmad, W. Mohd Ashri, W. Daud, A. Azmier, R.R. Mohd, Using cocoa (*Theobroma cacao*) shell-based activated carbon to remove 4-nitrophenol from aqueous solution: kinetics and equilibrium studies, Chem. Eng. J. 178 (2011) 461–467.
[26] A. Derylo-Marczewska, B. Buczek, A. Swiatkowski, Effect of oxygen surface groups on adsorption of benzene derivatives from aqueous solutions onto active carbon samples, Appl. Surf. Sci. 257 (2011) 9466–9472.
[27] B.H. Hameed, A.A. Rahman, Removal of phenol from aqueous solutions by adsorption onto activated carbon prepared from biomass material, J. Hazard. Mater. 160 (2008) 576–581.
[28] S. Dutta, J.K. Basu, R.N. Ghar, Studies on adsorption of p-nitrophenol on charred saw-dust, Sep. Purif. Technol. 21 (2001) 227–235.
[29] M.H. Entezari, Z. Sharif Al-Hoseini, N. Ashraf, Fast and efficient removal of Reactive Black 5 from aqueous solution by a combined method of ultrasound and sorption process, Ultrason. Sonochem. 151 (2008) 433–437.
[30] M.H. Entezari, Z. Sharif Al-Hoseini, Sono-sorption as a new method for the removal of methylene blue from aqueous solution, Ultrason. Sonochem. 14 (2007) 599–604.
[31] O. Hamdaoui, E. Naffrechoux, Adsorption kinetics of 4-chlorophenol onto granular activated carbon in the presence of high frequency ultrasound, Ultrason. Sonochem. 16 (2009) 15–22.
[32] B.S. Schueller, R.T. Yang, Ultrasound enhanced adsorption and desorption of phenol on activated carbon and polymeric resin, Ind. Eng. Chem. Res. 40 (2001) 4912–4918.
[33] Z. Wang, K.L. Cheng, Effect of ultrasound and mechanical agitation on adsorption of PAR by Amberlite XAD-2, Ultrasonics 20 (1982) 215–216.
[34] J. Hristov, L. Fachikov, An overview of separation by magnetically stabilized beds: state-of-the-art and potential applications, Chin. Particuol. 5 (2007) 11–18.
[35] R.D. Max, M.B. Jefferson, A. Simon, P. Peter Jarvis, Magnetic ion-exchange resin treatment: Impact of water type and resin use, Water Res. 42 (2008) 1977–1988.
[36] L.C.A. Oliveira, D.I. Petkowicz, A. Smaniotto, S.B.C. Pergher, Magnetic zeolites: a new adsorbent for removal of metallic contaminants from water, Water Res. 38 (2004) 3699–3704.
[37] L. Zhang, X. Zhu, S. Zheng, H. Sun, Photochemical preparation of magnetic chitosan beads for immobilization of pullulanase, Biochem. Eng. J. 46 (2009) 83–87.
[38] P.I. Girginova, A.L. Daniel-da-Silva, C.B. Lopes, P. Figueira, M. Otero, V.S. Amaral, E. Pereira, T. Trindade, Silica coated magnetite particles for magnetic removal of Hg^{2+} from water, J. Colloid Interface Sci. 345 (2010) 234–240.
[39] P. Panneerselvam, N. Morad, K.A. Tan, Magnetic nanoparticle (Fe_3O_4) impregnated onto tea waste for the removal of nickel(II) from aqueous solution, J. Hazard. Mater. 186 (2011) 160–168.
[40] A.B. Fueretes, P. Tartaj, A facile route for the preparation of superparamagnetic porous carbons, Chem. Mater. 18 (2006) 1675–1679.
[41] A. Nakahira, H. Nagata, M. Takimura, K. Fukunishi, Synthesis and evaluation of magnetic active charcoals for removal of environmental endocrine disrupter and heavy metal ion, J. Appl. Phys. 101 (2007) 09J114–09J116.
[42] L.C.A. Oliveira, R.V.R.A. Rios, J.D. Fabris, V. Garg, K. Sapag, R.M. Lago, Activated carbon/iron oxide magnetic composites for the adsorption of contaminants in water, Carbon 40 (2002) 2177–2183.
[43] M. Schwickardi, S. Olejnik, E.-L. Salabas, W. Schmidt, F. Schüth, Scalable synthesis of activated carbon with superparamagnetic properties, Chem. Commun. (2006) 3987–3989.
[44] G.S. Zhang, J.H. Qu, H.J. Liu, A.T. Cooper, R.C. Wu, $CuFe_2O_4$/activated carbon composite: a novel magnetic adsorbent for the removal of acid orange II and catalytic regeneration, Chemosphere 68 (2007) 1058–1066.
[45] Y. Ao, J. Xu, D. Fu, X. Shen, C. Yuan, A novel magnetically separable composite photocatalyst: titania-coated magnetic activated carbon, Sep. Purif. Technol. 61 (2008) 436–441.
[46] N. Atsushi, S. Nishida, K. Fukunishi, Synthesis of magnetic activated carbons for removal of environmental endocrine disrupter using magnetic vector, J. Ceram. Soc. Jpn. 114 (2006) 135–137.
[47] S. Brunauer, P. Emmett, E. Teller, Adsorption of gases in multimolecular layers, J. Am. Soc. 60 (1938) 309–319.
[48] B.D. Cullity, Elements of X-Ray Diffraction, second ed., Addison Wesley, 1978.
[49] J.S. Noh, J.A. Schwarz, Estimation of the point of zero charge of simple oxides by mass titration, J. Colloid Interface Sci. 130 (1989) 157–164.
[50] H.P. Boehm, Some aspects of the surface chemistry of carbon blacks and other carbons, Carbon 32 (1994) 759–769.
[51] T. Rohani Bastami, M.H. Entezari, A novel approach for the synthesis of superparamagnetic Mn_3O_4 nanocrystals by ultrasonic bath, Ultrason. Sonochem. 19 (2012) 560–569.
[52] T. Rohani Bastami, M.H. Entezari, Synthesis of manganese oxide nanocrystal by ultrasonic bath: effect of external magnetic field, Ultrason. Sonochem. 19 (2012) 830–840.
[53] Y. Ao, J. Xu, X. Shen, D. Fu, C. Yuan, Magnetically separable composite photocatalyst with enhanced photocatalytic activity, J. Hazard. Mater. 160 (2008) 295–300.
[54] S. Brunauer, L.S. Deming, W.E. Deming, E. Teller, On a theory of the van der waals adsorption of gases, J. Am. Chem. Soc. 62 (1940) 1723–1732.
[55] K.S.W. Sing, D.H. Everett, R.H.W. Haul, L. Moscou, R.A. Oierotti, J. Rouquerol, T. Siemieniewska, International union of pure and applied chemistry physical chemistry division commission on colloid and surface chemistry including catalysis, Pure Appl. Chem. 57 (1985) 603–619.
[56] E.O. Augustine, Kinetics and pseudo-isotherm studies of 4-nitrophenol adsorption onto mansonia wood sawdust, Ind. Crop. Prod. 33 (2011) 418–428.
[57] T.J. Mason, Practical Sonochemistry: User's Guide to Applications in Chemistry and Chemical Engineering, Ellis Horwood, Chichester, 1991.
[58] L.H. Thompson, L.K. Doraiswamy, Sonochemistry: science and engineering, Ind. Eng. Chem. Res. 38 (1999) 1215–1249.
[59] Y.S. Ho, J.C.Y. Ng, G. Mckay, Removal of lead(II) from effluents by sorption using second order kinetics, Sep. Sci. Technol. 36 (2001) 241–261.
[60] N. Sivakumar, K. Min, Phenolic compounds biosorption onto Schizophyllum commune fungus: FTIR analysis, kinetics and adsorption isotherms modeling, Chem. Eng. J. 168 (2011) 562–571.
[61] Y.S. Ho, G. McKay, Sorption of dye from aqueous solution by peat, Chem. Eng. J. 70 (1998) 115–124.
[62] S.B. Harogoppad, T.M. Aminabhavi, Diffusion and sorption of organic liquids through polymer membranes. II. Neoprene, SBR, EPDM, NBR and natural rubber versus n-alkanes, J. Appl. Polym. Sci. 42 (1991) 2329–2336.